RMetS

Royal Meteorological Society

Diagnosing the vertical structure of the eddy diffusivity in real and idealized atmospheres

Malte Jansen[a]* and Raffaele Ferrari[b]

[a]*Geophysical Fluid Dynamics Laboratory, Princeton, NJ, USA*
[b]*Massachusetts Institute of Technology, Cambridge, USA*

*Correspondence to: M. Jansen, Geophysical Fluid Dynamics Laboratory, 201 Forrestal Rd, 303B, Princeton, NJ 08544, USA.
E-mail: mjansen@princeton.edu*

The Earth's extratropical troposphere is equilibrated by turbulent eddy fluxes of potential temperature and momentum. The equilibrated state has the remarkable characteristic that isentropic slopes leaving the surface in the subtropics reach the tropopause near the Poles. It has been speculated that turbulent eddy fluxes maintain this state for a wide range of radiative forcing and planetary parameters. In a previous study, the authors showed that this state needs to be associated with an eddy diffusivity of Ertel potential vorticity that is largest at the surface and decays through the troposphere to approximately zero at the tropopause. This result is confirmed in this study using atmospheric reanalysis and idealized numerical simulations. However, it is also shown that the vertical profile of the eddy diffusivity can change, resulting in different isentropic slopes and climates. This is illustrated with a series of idealized numerical simulations with varying planetary scales and rotation rates.

1. Introduction

A major issue for climate studies is to understand how turbulent eddy fluxes maintain the observed atmospheric mean state. Observations suggest that the time- and zonal-mean state of the extratropical atmosphere is equilibrated such that isentropes leaving the surface in the subtropics reach the tropopause near the poles, and thus $\xi \sim (a/H)s \sim \mathcal{O}(1)$, where s denotes a characteristic isentropic slope, H denotes the depth-scale of the troposphere and a is the planetary radius. The parameter ξ (in this or related formulations) is commonly referred to as the criticality parameter, since the condition that $\xi \sim \mathcal{O}(1)$ bears a resemblance to the marginal criticality condition in the two-layer quasi-geostrophic (QG) model, where small criticality parameters denote a state that is stable to baroclinic instability while large criticality parameters denote a strongly unstable state (Stone, 1978).

Various previous studies have argued that the criticality parameter is related to the vertical structure of the eddy fluxes (Green, 1970; Held, 1978, 1982; Schneider, 2004; Jansen and Ferrari, 2013b). Using a constraint on the vertically integrated zonal momentum budget, Held (1978, 1982) argued that atmospheric mean states with $\xi \approx 1$ are obtained if the eddy flux of potential vorticity (PV) decays to zero in the vertical over the depth-scale of the troposphere.

If the eddy fluxes of PV are down the mean gradient, an eddy diffusivity can be defined and one can more generally formulate a relation between the mean isentropic slope and the vertical structure of the eddy diffusivity over the depth of the troposphere (Green, 1970). The result suggests that,

for any finite criticality parameter ξ, the eddy diffusivity needs to decay in the vertical over the depth of the troposphere. Mean states with $\xi \approx 1$ are obtained if the eddy diffusivity decays from its surface value to about zero near the tropopause.

The relevance of the QG results of Green (1970) and Held (1978) to the real atmosphere has been questioned by Schneider (2004). He argued that, in primitive equations, mean states with $\xi \sim \mathcal{O}(1)$ arise if the eddy diffusivity is approximately constant throughout the whole depth of the troposphere. Schneider and Walker (2006) moreover surmised that, as a consequence, strongly supercritical mean states may be impossible in primitive equations. The reasoning is that eddies should become essentially barotropic in highly supercritical flows (Rhines, 1977; Salmon, 1978, 1980; Held and Larichev, 1996). This in turn would justify the assumption that the eddy diffusivity is vertically constant. According to Schneider (2004), however, a vertically constant eddy diffusivity would result in a marginally critical mean state, leading to a contradiction with the assumption of a strongly supercritical state.

The derivation of Schneider (2004) has recently been challenged by Jansen and Ferrari (2013b), who instead showed that the QG results are recovered in primitive equations if isentropic averages are defined appropriately. Moreover, a growing number of recent studies have found that supercritical mean states can indeed be obtained in numerical simulations of primitive equation atmospheres (e.g. Zurita-Gotor, 2008; Zurita-Gotor and Vallis, 2010; Jansen and Ferrari, 2012, 2013a).

Jansen and Ferrari (2013b) derived a relation between the criticality parameter and the vertical structure of the

eddy diffusivity:

$$\xi \sim \frac{[D]}{\Delta D}, \qquad (1)$$

where $[D]$ is the vertical mean of the tropospheric eddy diffusivity and ΔD is the bulk difference between the eddy diffusivities in the lower and upper troposphere. The derivation of Eq. (1) will be sketched in section 3. The main implication of this result is that strongly supercritical states ($\xi \gg 1$) can have eddy diffusivities approximately constant throughout the whole depth of the troposphere, consistent with the expectation of strong barotropization in this limit. Mean states close to marginal criticality (i.e. $\xi \approx 1$), as found in the Earth's extratropical atmosphere, instead require the eddy diffusivity to decay strongly over the depth of the troposphere.

This study analyzes the vertical structure of the eddy diffusivity in the troposphere and tests the relationship in Eq. (1). Eddy diffusivities are computed directly from the flux gradient relationships of PV and surface potential temperature, the two variables that enter in the theoretical arguments. Since the Earth's extratropical troposphere is in a state near marginal criticality, Eq. (1) requires that the eddy diffusivity decays substantially over the depth of the troposphere. This will be confirmed by atmospheric reanalysis data, which show that the extratropical eddy diffusivity decays from large values near the surface to almost zero near the tropopause.

To test the scaling relation in Eq. (1) more quantitatively, we will analyze the vertical structure of the eddy diffusivity in a series of idealized numerical simulations first presented in Jansen and Ferrari (2013a). By varying the Coriolis parameter f and planetary vorticity gradient β in an idealized primitive equation model, a large range of climate states can be obtained, with criticality parameters ranging from $\xi \sim \mathcal{O}(1)$ to $\xi \sim O(10)$. In this article, we will first confirm that these simulations indeed produce weakly nonlinear flows for mean states with $\xi \sim \mathcal{O}(1)$, while the flows exhibit all properties of fully developed geostrophic turbulence when $\xi \sim \mathcal{O}(10)$. The simulations are then used to confirm the scaling relation between the criticality parameter and the vertical structure of the eddy diffusivity in Eq. (1).

This article is organized as follows. In section 2, we present an analysis of the isentropic eddy diffusivities of PV from reanalysis data. The theoretical arguments for the relation between the criticality parameter and the vertical structure of the eddy diffusivity are sketched in section 3. In section 4, we use the results of a series of numerical simulations to test quantitatively the relation between the criticality parameter and the vertical structure of the eddy diffusivity. Some concluding remarks are presented in section 5.

2. Observations

It seems appropriate to begin by diagnosing from observations the vertical structure of the eddy diffusivity in the extratropical atmosphere. Haynes and Shuckburgh (2000) estimated tropospheric and lower stratospheric eddy diffusivities advecting a passive tracer with re-analyzed velocity fields and using the effective diffusivity diagnostic proposed by Nakamura (1996). Their results suggest that the extratropical eddy diffusivity decays strongly between the 300 K surface and the tropopause, in qualitative agreement with the argument of Green (1970) and Jansen and Ferrari (2013b), who predict a vertical decrease in the eddy diffusivity. Unfortunately, the analysis of Haynes and Shuckburgh (2000) does not extend below the 300 K surface and thus misses a significant part of the extratropical lower troposphere. Furthermore, the calculation is based on Nakamura's (1996) effective diffusivity diagnostic, rather than a local relation between the eddy PV flux and gradient, as assumed in the theoretical arguments leading to Eq. (1).

We here estimate the eddy diffusivity of PV and surface potential temperature directly from the ratio of the respective eddy fluxes and mean gradients from the ERA-40 reanalysis (Kållberg *et al.*, 2004). The reanalysis data are particularly useful for the task, since they combine available observations with a physical model that enforces dynamical consistency. All fluxes and gradients are computed as averages over the time period from 1982–2000. For simplicity, we will only discuss annual averages, but qualitatively similar results are obtained for each season.

For near-adiabatic flows, eddies mix Ertel PV along isentropic surfaces, thus generating a net down-gradient flux of PV. To estimate the eddy diffusivity, we thus compute eddy fluxes and gradients of PV along isentropic surfaces.* Time and zonal averages along isentropes are computed as proposed by Koh and Plumb (2004). A thickness-weighted average is defined as $\overline{()}^* = \overline{\mathcal{H}(\theta - \theta_s)\partial_\theta p()} / \overline{\mathcal{H}(\theta - \theta_s)\partial_\theta p}$, where the overbar denotes a time and zonal mean on an isentropic surface, $\partial_\theta p$ denotes the isentropic 'thickness' (the pressure difference between two isentropic surfaces) and $\mathcal{H}(\theta - \theta_s)$ is the Heaviside function, with θ_s the surface potential temperature. The Heaviside function in the definition of the generalized thickness-weighted average takes care that averages are taken only over the regions where the isentropic surface is above the ground. Deviations from the thickness-weighted isentropic average are denoted by a hat, i.e. $\hat{()} = () - \overline{()}^*$.

A problem arises when calculating isentropic diagnostics from atmospheric data: the stratification is frequently statically unstable in the planetary boundary layer. A dynamically meaningful coordinate transformation from model levels into isentropic coordinates requires that $\theta(p)$ be monotonic. To avoid this problem, we ignore the 10 lowest model levels[†] of the reanalysis data, which comprise the lowest $\sim$1.1 km above the surface, where virtually all of the negative $\partial_p \theta$ occur. Averages on isentropes that intersect with this boundary layer are treated as discussed above, but with the surface potential temperature θ_s replaced by the potential temperature at the top of this layer.

If eddy fluxes are assumed to be nearly adiabatic (we will return to this assumption below), we expect the meridional isentropic eddy PV flux to be down the mean gradient (e.g. Jansen and Ferrari, 2013b), thus justifying the definition of an isentropic PV diffusivity as

$$D \equiv -\frac{\overline{\hat{v}\hat{P}}^*}{\partial_y \overline{P}^*}. \qquad (2)$$

Here, v is the meridional velocity and $P \equiv (f + \zeta)/(g^{-1}\partial_\theta p)$ is the Ertel PV, where $\zeta = \partial_x v - \partial_y u$ is the relative vorticity, with derivatives taken along θ surfaces.

Near the surface, we expect eddies to flux potential temperature horizontally down its mean-gradient. In the interior, the potential temperature flux is mostly skewed, i.e. it is dominated by the advection by a generalized Stokes drift, with a smaller diffusive component. Along the surface, however, the flux is diffusive, because the Stokes drift has to vanish due to the no-normal-flow boundary condition. It is thus justified to define an eddy diffusivity for near-surface potential temperature as

$$D_s \equiv -\frac{\overline{v'\theta'}^s}{\partial_y \overline{\theta}^s}, \qquad (3)$$

---

*Isentropic coordinate diagnostics are computed after vertically interpolating the four-hourly data from the model grid ($\approx 1.12° \times 1.12°$, 60 vertical hybrid levels) on to 120 isentropic surfaces. We interpolate integral quantities (integrated from the surface to a given level) linearly, which guarantees that integral budgets are not affected by the interpolation. *In situ* quantities on isentropes are then obtained by differentiating the interpolated integral quantities vertically. The original script used to compute the isentropic diagnostics was kindly provided by Christopher Walker and was slightly modified.

†The model uses a hybrid coordinate system. The pressure at the top of the tenth model level is given as $p = 3850.91\,\text{Pa} + 0.847375 \times p_s$, where p_s denotes the local surface pressure.

(a) $\overline{\rho_\theta \hat{v} \hat{P}}$

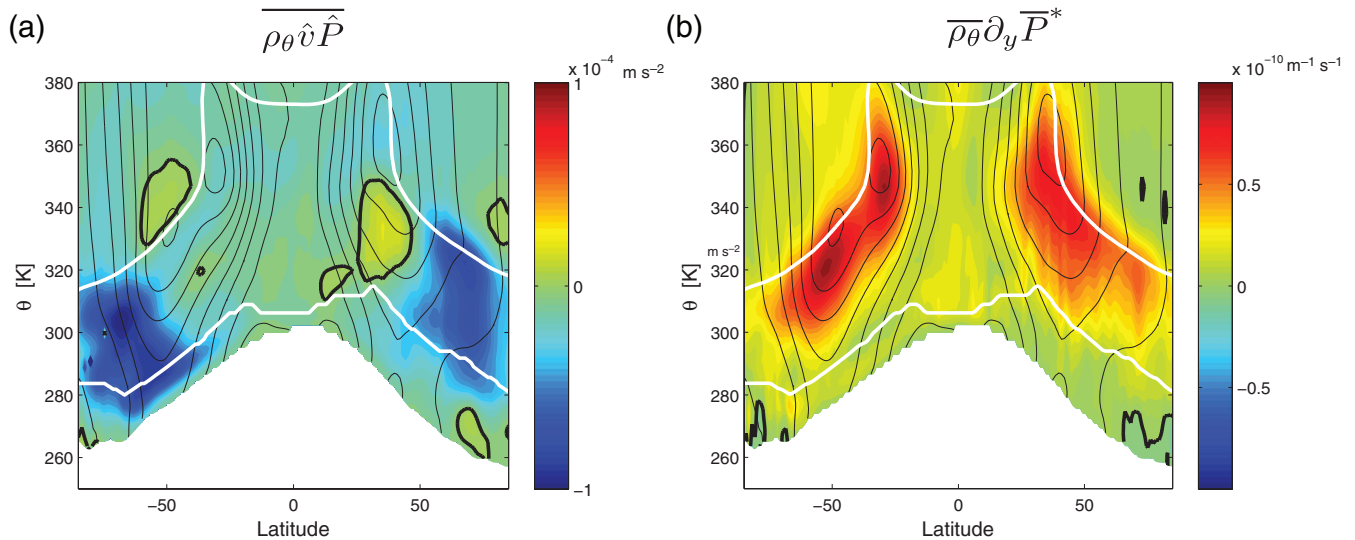(b) $\overline{\rho_\theta \partial_y \overline{P}^*}$

Figure 1. (a) Thickness-weighted isentropic PV fluxes, $\overline{\rho_\theta \hat{v} \hat{P}}$, from the ERA-40 reanalysis (colour shading). The thick black contours denote zero PV flux. The thin black contours show the zonal mean zonal wind. The white lines indicate the top of the surface layer (here defined by the 95% quantile of potential temperature at the top of the boundary layer) and the tropopause (defined by a lapse rate of $dT/dz = 2\,\mathrm{K\,km^{-1}}$). (b) As (a), but showing the thickness-weighted isentropic PV gradient, $\overline{\rho_\theta \partial_y \overline{P}^*}$.

where $\overline{(\,)}^s$ denotes an average along the top of the boundary layer, as defined above, and primes denote deviations from this average.

Figure 1 shows the isentropic mean PV gradient and eddy PV flux as a function of latitude and θ. The PV gradient is primarily associated with the planetary vorticity gradient, β, which is positive everywhere, and a contribution associated with the thickness gradient, $\partial_y \partial_\theta p$, which is also positive throughout most of the troposphere and is particularly large near the tropopause, because the isentropic thickness decreases strongly when isentropes intersect with the tropopause. As a result, the PV gradient is positive throughout almost all of the troposphere and largest near the tropopause. The PV flux is mostly negative throughout the troposphere, in agreement with the notion of generally down-gradient eddy fluxes. Weak up-gradient PV fluxes, however, can be seen locally around the subtropical jet, a feature that has recently been discussed in detail by Birner *et al.* (2013).

The resulting isentropic eddy PV diffusivity, calculated according to Eq. (2), is shown in Figure 2. Outside the aforementioned regions around the subtropical jets, the eddy diffusivity is positive but varies spatially. As discussed in the Introduction, we are especially interested in the vertical structure of the eddy diffusivity in the extratropics. The eddy diffusivity decays strongly towards the upper troposphere, as suggested by Green (1970) and Jansen and Ferrari (2013b).

In addition to the isentropic eddy PV diffusivity, Figure 2 shows the near-surface eddy potential temperature diffusivity, calculated according to Eq. (3). Over the extratropics, where PV and buoyancy fluxes are dominated by geostrophic eddies, the near-surface potential temperature diffusivity is of similar magnitude to the isentropic eddy PV diffusivity near the surface.[‡] This result is encouraging, since the eddy diffusivity is expected to be a fundamental property of the flow, describing the rate of mixing by the turbulent eddies independently of the tracer being stirred. The result is also in agreement with the numerical results discussed in Jansen and Ferrari (2013b).

Notice that the local diffusive closure in Eq. (2) is physically well justified only in the limit where the fluxes of PV variance
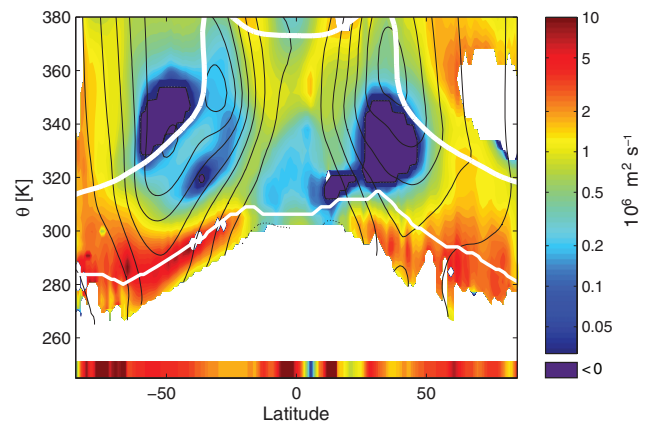

Figure 2. Estimate of the isentropic eddy PV and near-surface potential temperature diffussivities from ERA-40 reanalysis data. The near-surface eddy diffusivity of potential temperature is represented by the bar at the bottom. The figure is cut off below the 5% quantile of the near-surface potential temperature (defined as the potential temperature at the top of the removed boundary layer) and the thin white line shows the 95% quantile of the near-surface potential temperature. The thick white line denotes an estimate of the tropopause (here calculated as the level where the stratification reaches $-2\mathrm{K\,km^{-1}}$). Notice that the colour bar is logarithmic. The purple shading denotes regions where the diffusivity becomes weakly negative.

are negligible and diabatic effects are small on the time-scale of eddy stirring (e.g. Jansen and Ferrari, 2013b). These assumptions, which are implied in the arguments of Schneider (2004) and Jansen and Ferrari (2013b), may not hold in the Earth's atmosphere, where geostrophic eddy statistics are strongly inhomogeneous and radiative forcing and latent heat release may affect eddy PV perturbations significantly . If these assumptions break down, the eddy diffusivity, as defined by Eq. (2), may not be positive definite or independent of the considered tracer.

Support for a diffusive closure is given by the result that the diffusivity as defined by Eq. (2) is dominantly positive. At the same time, the regions of negative diffusivities near the subtropical jets show that, locally, the assumptions required for a down-gradient flux closure break down. Birner *et al.* (2013) show that these up-gradient fluxes are associated with significant horizontal fluxes of PV variance. Notice that these fluxes vanish upon integration in the horizontal, suggesting that diffusive closures are more appropriate when used as a description of the large-scale averaged fluxes.

[‡]Notice that the eddy PV diffusivity varies significantly throughout the depth of the surface layer and becomes poorly defined towards its bottom (which comprises potential temperature values that are only rarely found at the given latitude). The bulk PV diffusivity, integrated over the surface layer, however, agrees very well with the near-surface eddy diffusivity of surface potential temperature everywhere outside the tropics and at latitudes with large topography (not shown).

Further encouragement is provided by the qualitative similarity between the PV diffusivities shown in Figure 2 and the effective diffusivity variations reported in Haynes and Shuckburgh (2000). There are, however, a few notable differences between the two diffusivity diagnostics. While the eddy PV diffusivity calculated from the flux/gradient ratio shows regions of weakly negative diffusivities near the subtropical jets, the effective diffusivity diagnostic calculated by Haynes and Shuckburgh (2000) is by construction positive everywhere. Furthermore, the regions of vanishingly small eddy PV diffusivities in Figure 2 seem to extend further downwards into the troposphere than the effective diffusivity minima reported in Haynes and Shuckburgh (2000).

Some differences are expected between the eddy PV diffusivity computed from a flux/gradient relationship and the effective diffusivity diagnostic, even if PV behaves identically to a passive scalar. From the perspective of the PV variance budget (e.g. Jansen and Ferrari, 2013b), the former represents the generation of variance, while the latter represents the dissipation of variance by irreversible mixing. The two quantities balance locally if and only if the advection of variance, as well as the dissipation by diabatic processes, can be neglected. Both variance advection and diabatic processes, however, may be significant in parts of the atmosphere (e.g. Birner *et al.*, 2013). Finally, the effective diffusivity diagnostic considers zonal averages along tracer contours, which are then mapped on to equivalent latitudes, while our results show averages taken at fixed latitude. Despite these differences, the main result of an eddy diffusivity that decays strongly from the surface towards the tropopause appears to be robust.

3. Theory

This article aims to test the relation between the criticality parameter and the vertical structure of the eddy diffusivity in Eq. (1). A heuristic derivation of this relationship is here derived using a continuously stratified QG model; this case was first discussed by Green (1970). For a more general derivation, using the primitive equations in isentropic coordinates, the reader is referred to Jansen and Ferrari (2013b).

We start from the inviscid time- and zonal-mean zonal momentum balance, which in the QG transformed Eulerian mean (TEM) formulation can be written as

$$-f_0 \bar{v}^* = \overline{v'q'}, \tag{4}$$

where

$$q = f_0 + \beta y + \partial_x v - \partial_y u + \frac{f_0}{\rho_0} \partial_z \frac{\rho_0 \theta}{\partial_z \theta_0}$$

is the QG PV,

$$\bar{v}^* = -\frac{1}{\rho_0} \partial_z (\rho_0 \psi^*)$$

is the residual meridional velocity, with the residual stream function

$$\psi^* \equiv -\frac{1}{\rho_0} \int_0^z \rho_0 \bar{v} \, dz' + \frac{\overline{v'\theta'}}{\partial_z \theta_0}$$

and the reference potential temperature and density profiles $\theta_0(z)$ and $\rho_0(z)$. Overbars denote time and zonal averages taken at constant z, which here denotes the log pressure height $z = -H \ln p/p_R$, with H the scale height and p_R a constant reference pressure. Primes denote deviations from this average. We can integrate Eq. (4) from the surface (for simplicity assumed to be flat[§] at $z = 0$) to the tropopause at $z = z_t$, where the residual

§In log pressure coordinates, we are technically assuming the bottom boundary to be a surface of constant pressure. Relaxing this assumption, however, would not alter the results discussed here in any significant way.

overturning stream function is assumed to vanish:

$$0 = \rho_0 \psi^*(z_t) = \int_0^{z_t} \frac{\rho_0 \overline{v'q'}}{f_0} \, dz' + \rho_0(0) \frac{\overline{v'\theta'}}{\partial_z \theta_0}(0), \tag{5}$$

where we used the fact that $\psi^*(0) = [\overline{v'\theta'}/\partial_z \theta_0](0)$. Equation (5) predicts a balance between the vertically integrated QG PV flux and the eddy flux of surface potential temperature.

A relation analogue to Eq. (5) can be derived for the primitive equations in isentropic coordinates (Koh and Plumb, 2004; Schneider, 2005; Jansen and Ferrari, 2013b), where one obtains

$$0 \approx -\int_{\theta_b}^{\bar{\theta}_t} \overline{\rho_\theta} \, \bar{v}^* \, d\theta \approx \int_{\theta_b}^{\bar{\theta}_t} \frac{\overline{\rho_\theta \hat{v} \hat{P}}^*}{\overline{P}^*} \, d\theta + \frac{f}{\overline{P}^*(\overline{\theta}^s)} \overline{v_g' \theta'}^s. \tag{6}$$

Here θ_b denotes the minimum potential temperature occurring in the domain and θ_t denotes the potential temperature at the tropopause. $\rho_\theta \equiv g^{-1} \mathcal{H}(\theta - \theta_s) \partial_\theta p$ denotes a generalized 'density' in isentropic coordinates, with the Heaviside function $\mathcal{H}(\theta - \theta_s)$, setting $\rho_\theta = 0$ on isentropes below the surface (i.e. where $\theta < \theta_s$). v_g denotes the geostrophic meridional velocity and $\overline{(\ )}^s$ denotes a time and zonal average along the surface.

The balance in Eq. (6) is illustrated for the atmospheric reanalysis in Figure 3. In agreement with the dominantly negative PV flux in Figure 1, we see an equatorward isentropic mass transport associated with the interior eddy PV flux, which is largely balanced by a poleward contribution associated with the eddy potential temperature flux at the top of the boundary layer. The two contributions, however, are not exactly equal and opposite. There is a significant residual, which is mostly due to the missing poleward transport in the frictional boundary layer; the analysis does not include the lowest ten model levels, which cover the atmospheric boundary layer. The mass transport in this boundary layer is associated primarily with the Ekman transport (maintained by frictional drag) and the geostrophic transport maintained by mountain drag. The magnitude of the missing transport in the boundary layer is consistent with estimates of the net frictional and mountain drag in the atmosphere (e.g. Oort and Peixóto, 1983).[¶] Some disagreement between these estimates and the residual transport shown in Figure 3 remains in the latitudinal pattern, in particular in the Northern Hemisphere. This is expected, due to differences in the underlying models as well as shortcomings in some of the approximations that entered into the derivation of Eq. (6), which are expected to be less accurate in the presence of significant topography. We are here interested only in the qualitative implications of Eq. (6) for the gross vertical structure of the eddy diffusivity. A detailed discussion of the role of friction and mountain drag in the planetary boundary layer is thus left for future studies.

Assuming a diffusive closure for the eddy fluxes of PV and surface potential temperature, i.e.

$$\overline{v'q'} = -D \partial_y \bar{q} \quad \text{and} \quad \overline{v'\theta'}(0) = -D_s \partial_y \bar{\theta}(0), \tag{7}$$

and ignoring the contribution of relative vorticity to the PV, Eq. (5) yields

$$\int_0^{z_t} D \left(\rho_0 \frac{\beta}{f_0} - \partial_{z'}(\rho_0 s) \right) dz' - \rho_0(0) D_s s(0) = 0. \tag{8}$$

Here $s \equiv -\partial_y \bar{\theta}/\partial_z \theta_0$ denotes the isentropic slope, $D = D(z)$ is the eddy PV diffusivity and D_s is the surface eddy buoyancy

¶Oort and Peixóto (1983) estimate the net mean drag due to bottom friction and mountain drag to have a maximum absolute value of about 1 dyn cm^{-2} = 10^{-1} kg (m s^2)$^{-1}$ at about 45°S. To obtain an estimate for the associated zonal mean mass transport as computed here, this needs to be divided by the Coriolis parameter $f(45°) \approx 10^{-4}$ s^{-1}. This yields an estimated transport of about 1000 kg (ms)$^{-1}$, which is of the same order of magnitude as the missing transport inferred from Figure 3.
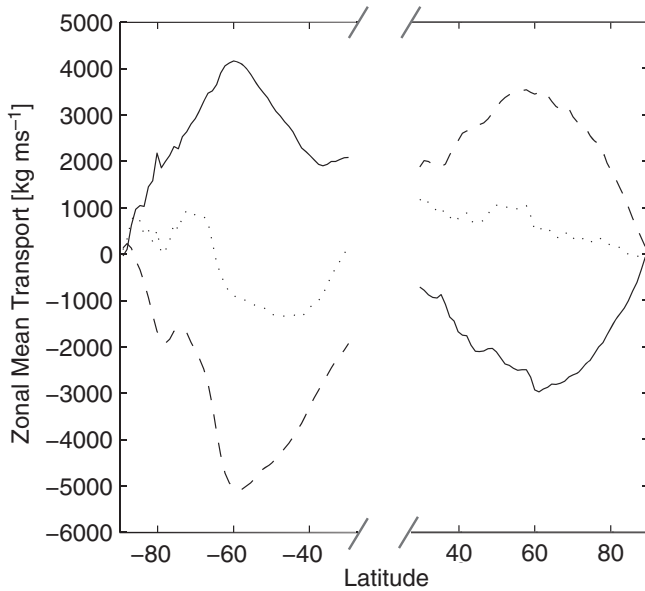
Figure 3. Net isentropic mass transport associated with the interior eddy PV flux $\int_{\theta_b}^{\bar{\theta}_t} \overline{\rho_\theta \hat{v} \hat{P}}^*/\overline{P}^* \, d\theta$ (solid) and the eddy flux of potential temperature at the top of the boundary layer $f/\overline{P}^*(\overline{\theta}^s) \, \overline{\hat{v}\hat{\theta}}^s$ (dashed), from the ERA-40 reanalysis. The dotted line shows the residual between the two, which is associated primarily with the missing mass transport in the boundary layer (see text).

diffusivity. If the eddy diffusivity is a fundamental property of the flow and independent of the tracer under consideration, we expect that $D_s = D(0)$. This was confirmed by the simulations discussed in Jansen and Ferrari (2013b), and is also supported qualitatively by the reanalysis data shown in Figure 2. Equation (8) can then be written as

$$\int_{0^-}^{z_t} D\left(\rho_0 \frac{\beta}{f_0} - \partial_{z'}(\mathcal{H}(z')\rho_0 s)\right) dz' = 0, \quad (9)$$

where $\mathcal{H}(z')$ denotes the Heaviside function. The lower bound of the integral here is understood to be chosen such that it includes the lower boundary at $z = 0$ and thus the δ-function contribution arising from the evaluation of $\partial_{z'}\mathcal{H}(z')$. By absorbing the surface contribution in Eq. (8) into the integral in Eq. (9), we are effectively using Bretherton's (1966) generalized PV formulation. The argument of the integral in Eq. (9) is the generalized PV gradient, with the δ-function contribution that arises from the evaluation of $\partial_{z'}\mathcal{H}(z')$ representing the 'surface PV sheet', which replaces the inhomogeneous surface boundary condition (Bretherton, 1966).

Equation (9) provides an integral constraint relating the mean state to the vertical structure of the eddy diffusivity. To obtain a scaling relation, we want to separate the integral in Eq. (9) into lower and upper troposphere contributions and define bulk diffusivities for each of these layers, which allows us to write

$$D_1 \int_{0^-}^{z_1} \left(\rho_0 \frac{\beta}{f_0} - \partial_{z'}(\mathcal{H}(z')\rho_0 s)\right) dz' \quad (10)$$

$$+ D_2 \int_{z_1}^{z_t} \left(\rho_0 \frac{\beta}{f_0} - \partial_{z'}(\rho_0 s)\right) dz' = 0,$$

where D_1 and D_2 are the bulk diffusivities for the lower and upper troposphere, respectively. D_1 and D_2 can be defined formally as the vertical averages of the eddy diffusivity over the respective layer, weighted by the generalized PV gradient (see also Appendix A).

The level z_1 that separates the lower and upper troposphere may in principle be chosen freely. However, the bulk diffusivities D_1 and D_2 are poorly defined layer averages if the generalized PV gradient takes on large positive and negative values within one layer. The most reasonable choice, therefore, is to choose

z_1 as the level where the PV gradient changes sign. Figure 1 suggests that in the Earth's atmosphere the interior PV gradient is positive throughout the whole troposphere and thus the level that separates positive and negative generalized PV gradients is just above the surface. D_1 is thus to be understood as the eddy diffusivity near the surface. D_2, instead, is a measure of the eddy diffusivity primarily in the mid and upper troposphere, because the PV gradient (which enters as the weighting for the bulk diffusivity) is small in the lower troposphere.

The density-weighted isentropic slope at the tropopause, $\rho_0(z_t)s(z_t)$, is generally negligible compared with $\rho_0(z_1)s(z_1)$, because both the density and the isentropic slope decrease strongly towards the tropopause (e.g. Schneider, 2004). Equation (10) then yields

$$\left[D_1(p(0) - p(z_1)) + D_2(p(z_1) - p(z_t))\right] \frac{\beta}{f_0}$$

$$\approx (D_1 - D_2)g\rho_0(z_1)s(z_1), \quad (11)$$

where we further used that $\mathcal{H}(z)\rho_0 s|_{z=0^-} = 0$. Equation (11) can be formulated in terms of a relation between the criticality parameter and the vertical structure of the eddy diffusivity, as

$$\xi \equiv \frac{f_0 s}{\beta H} \sim \frac{[D]}{\Delta D}, \quad (12)$$

where $[D] \equiv ([p(0) - p(z_1)]D_1 + [p(z_1) - p(z_t)]D_2)/[p(0) - p(z_t)]$ is the vertical mean eddy diffusivity and $\Delta D \equiv D_1 - D_2$ is the difference between the bulk diffusivities in the lower and upper troposphere. The depth-scale H is here defined as $H = [p(0) - p(z_t)]/[g\rho_0(z_1)]$. For the Boussinesq fluid considered in the numerical simulations below, $\rho_0(z) = $ constant and and thus $H = z_t$.

Equation (12) states that the relative vertical variation of the eddy diffusivity scales inversely with the criticality parameter. $\mathcal{O}(1)$ criticality parameters are associated with a strong vertical decay in D. Strongly supercritical states are associated with weak vertical variations in D, which is in agreement with the fact that eddies tend to be more barotropic in the strongly supercritical limit (Rhines, 1977; Salmon, 1978, 1980; Held and Larichev, 1996). Jansen and Ferrari (2013b) discuss how the result in Eq. (12) can be generalized to primitive equations, using the isentropic momentum budget in Eq. (6). The results are summarized in Appendix A.

4. Numerical simulations

We now test the arguments discussed in the previous section by analyzing a series of numerical simulations with strongly varying criticality parameters. The simulations are the same as the ones discussed in Jansen and Ferrari (2013a).[∥] They use a primitive equation model in a β-plane channel configuration, where the Coriolis parameter varies as a linear function of latitude: $f = f_0 + \beta y$. This allows one to change the Coriolis parameter f_0 and the planetary vorticity gradient β separately and without changing the size of the domain. On a spherical planet, $f = 2\Omega \sin\phi$ and $\beta = a^{-1}\partial_\phi f = 2\Omega a^{-1}\cos\phi$, where Ω is the rotation rate, a is the planetary radius and ϕ denotes the latitude. The parameters f and β are therefore related through the planetary scale, such that in the midlatitudes $f/\beta \sim a$. In β-plane models, instead, it is possible to vary f_0 and β independently, without changing the size of the domain. It is the dynamical scale, f_0/β, that enters into the definition of the criticality parameter and thus determines the characteristics of the flow. Exploring various combinations of f_0 and β thus proves to be an efficient way to vary the criticality parameter of the equilibrated mean state greatly and thus test the theoretical arguments discussed above.

[∥]We here offer additional information about the simulations, since the description in Jansen and Ferrari (2013a) is very terse.
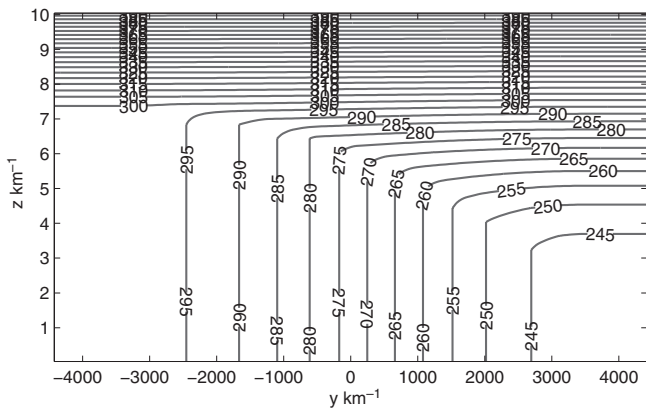
Figure 4. Equilibrium potential temperature for thermal restoring in K.

4.1.　Model set-up

We use a hydrostatic, Boussinesq, Cartesian coordinate configuration of the Massachusetts Institute of Technology (MIT) general circulation model (Marshall *et al.*, 1997). The set-up is very similar to the one discussed in Jansen and Ferrari (2013b): a zonally re-entrant β-plane channel, 15 000 km long, bounded meridionally by side walls at $y = \pm 4500$ km and vertically by a rigid lid at $z = H = 10.2$ km and a flat bottom at $z = 0$. Free slip boundary conditions are used on all boundaries and kinetic energy is removed by a linear Rayleigh drag with a constant drag coefficient of $r = (50 \, \text{day})^{-1}$ throughout the domain. We use a linear equation of state with a thermal expansion coefficient of $\alpha = 3.6 \times 10^{-4} \, \text{K}^{-1}$, i.e. $b = g\alpha(\theta - \theta_0)$, where b is buoyancy, θ_0 a reference potential temperature and g the acceleration of gravity. The thermal expansion coefficient used here is larger than that in Jansen and Ferrari (2013b) and was chosen to resemble the thermal expansion of air. The simulations are forced through relaxation to the equilibrium temperature profile shown in Figure 4. The relaxation time-scale is $\tau_s = 14$ days at the surface and decreases exponentially, with an e-folding depth of 500 m, to an interior value of $\tau_{int} = 50$ days. The reduced restoring time-scale near the surface is an idealized representation of the strong coupling of the lower troposphere to the surface temperature. It results in more realistic temperature profiles than obtained with the constant restoring time-scale used in Jansen and Ferrari (2013b). The simulations are spun up until a quasi-steady state is reached. Diagnostics are calculated over at least 500 days after equilibration is reached, which guarantees that the results presented are not affected by stochastic variability.

The set-up was chosen to provide an idealized test bed for the theory discussed and avoids various possibly complicating factors, such as processes associated with compressibility, convection, and a frictional boundary layer. While these processes can have a quantitative influence on the proposed relations, the qualitative results presented here should carry over to more realistic set-ups. We compared our results with the vertical structure of the eddy diffusivity obtained in simulations presented in Jansen and Ferrari (2012), which employ a more realistic radiative restoring profile and a frictional bottom boundary layer. Despite these differences, the results are qualitatively similar. A detailed analysis of the roles of the various neglected processes is left for future studies. Notice that the argument in Jansen and Ferrari (2013b), as well as the QG derivation in section 3, is for the general case of a compressible gas. The result for the Boussinesq limit, relevant for the presented simulations, is analogous and obtained by using $\rho_0 = $ constant and $dp \rightarrow \rho_0 g \, dz$.

4.2.　General results

We discuss a total of 11 simulations with Coriolis parameters $f_0 = 1, 2, 4, 8 \times 10^{-4} \, \text{s}^{-1}$ and planetary vorticity gradients $\beta = 0.8, 1.6, 3.2 \times 10^{-11} \, \text{m}^{-1} \, \text{s}^{-1}$. This allows for a total of

12 possible combinations of f_0 and β. Only the combination $f_0 = 1 \times 10^{-4} \, \text{s}^{-1}$, $\beta = 3.2 \times 10^{-11} \, \text{m}^{-1} \, \text{s}^{-1}$ was omitted, since the resulting Coriolis parameter $f = f_0 + \beta y$ would change sign within the domain. Such a sign change would give rise to a Hadley circulation regime, which is outside of the scope of this study.

We want to start by looking at the adjustment of the mean state by considering two illustrative cases: one using parameters characteristic for the Earth's midlatitudes: $f_0 = 1 \times 10^{-4} \, \text{s}^{-1}$, $\beta = 1.6 \times 10^{-11} \, \text{m}^{-1} \, \text{s}^{-1}$, and one using a much faster rotation rate, but less curvature: $f_0 = 8 \times 10^{-4} \, \text{s}^{-1}$, $\beta = 0.8 \times 10^{-11} \, \text{m}^{-1} \, \text{s}^{-1}$, which turns out to be the most supercritical simulation. Figure 5 shows snapshots of surface potential temperature as well as the equilibrated time and zonal mean state for both simulations. In the simulations with Earth-like parameters, eddies equilibrate the system in a way that qualitatively resembles the extratropical atmosphere in many aspects. In particular, we find that the isentropic slope is such that the criticality parameter is around 1, i.e. $s \sim \beta H/f_0$. The simulation develops a very pronounced westerly jet. As in the extratropical atmosphere, isentropic slopes are enhanced in the centre of the jet and are somewhat weaker outside.

The simulation with $f_0 = 8 \times 10^{-4} \, \text{s}^{-1}$, $\beta = 0.8 \times 10^{-11} \, \text{m}^{-1} \, \text{s}^{-1}$ instead equilibrates to a strongly supercritical mean state. Notice that f_0/β is here increased by a factor of 16 relative to the Earth-like case. A marginally critical state would thus require that the characteristic slope of the isentropes be decreased by a factor of 16, or that the tropopause height be increased by a similar amount (see Eq. (12)). As shown in Figure 5, this is clearly not the case. The isentropic slope is somewhat reduced compared with the simulation with Earth-like parameters, but the reduction is much weaker than predicted by adjustment to marginal criticality. The change in the average height of the troposphere is negligible.

Criticality parameters for all simulations are estimated as

$$\xi \equiv \frac{f_0}{\beta H} \frac{\langle \partial_y \theta \rangle}{\langle \partial_z \theta \rangle}, \tag{13}$$

where $\langle ( ) \rangle$ denotes a horizontal average over the entire baroclinically forced region $-3500 \, \text{km} < y < 3500 \, \text{km}$, taken at the fixed level $z = 2 \, \text{km}$ (which roughly corresponds to the average height of the layer interface used to calculate bulk diffusivities below). Notice that in some simulations the baroclinicity in this region varies relatively little and has only one maximum, while others have multiple distinct jets. The detailed jet structure does not affect the arguments tested in this study. The tropopause height varies little across our simulations, because it is tightly controlled by the radiative restoring profile (see Zurita-Gotor and Vallis, 2011, for a discussion of this constraint). For simplicity, we set $H = 7.5 \, \text{km}$ in Eq. (13) for all simulations.

The criticality parameters vary between 0.9 (for $f_0 = 1 \times 10^{-4}$, $\beta = 1.6 \times 10^{-11}$) and 8.8 (for $f_0 = 8 \times 10^{-4}$, $\beta = 0.8 \times 10^{-11}$) and are summarized in Table 1. The mean states thus range from marginally critical to strongly supercritical. We do not obtain any simulations that are strongly subcritical. The reason for this is discussed in Jansen and Ferrari (2013a), where we argue that geostrophic eddies can maintain strongly subcritical mean states only in the limit of extremely long radiative restoring time-scales.

The criticality parameter has important implications for the characteristics of the turbulent flow. In particular, criticality parameters larger than one are expected to be associated with strongly nonlinear flows, which produce a significant upscale energy transfer, resulting in eddies much larger than the scale of the linearly most unstable mode (Held and Larichev, 1996). As discussed in Appendix B, an analysis of the spectral energy budget confirms that, in the simulation with Earth-like rotational parameters, the scale of the instability and the scale of the most energetic eddies are very similar. The scale separation, however, increases approximately linearly with the criticality parameter, demonstrating the increasing role of nonlinear eddy–eddy
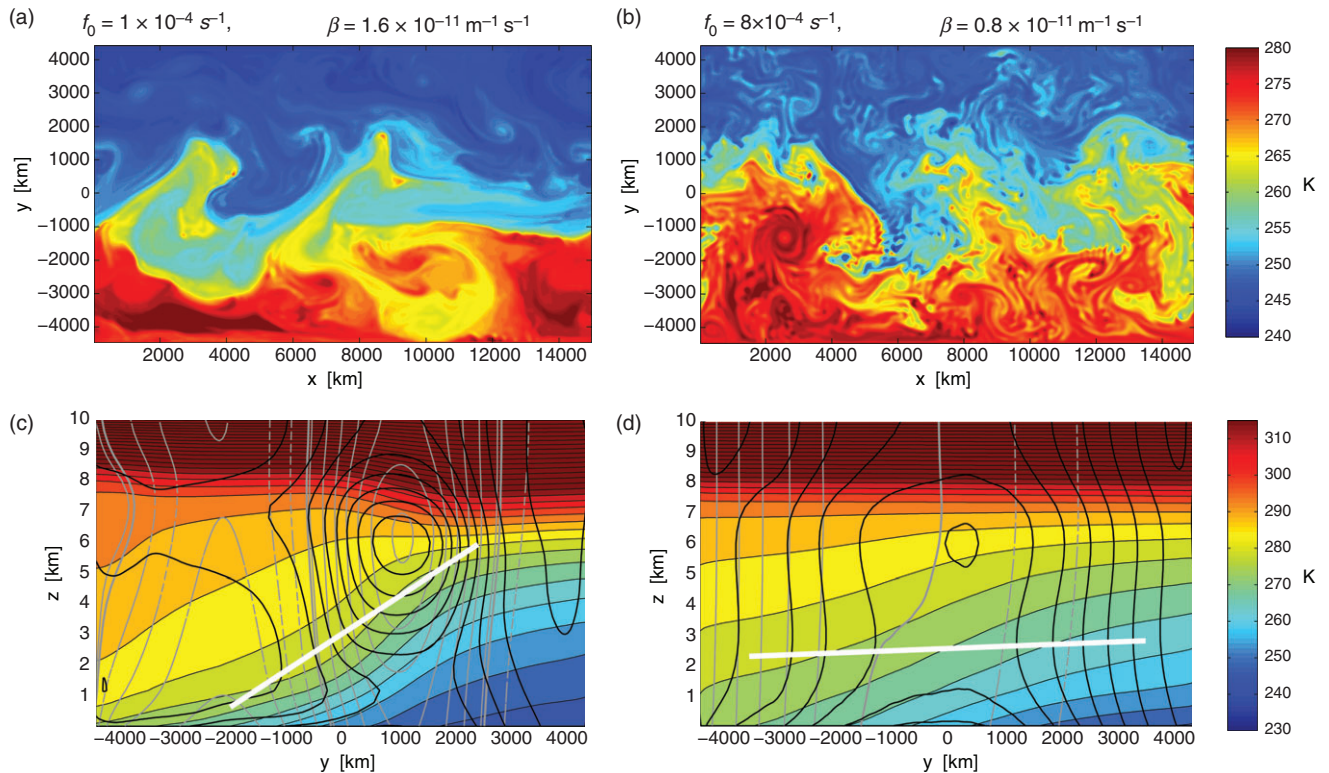
Figure 5. (a, b) Snapshots of surface potential temperature from the simulations with $f = 1 \times 10^{-4}$ s^{-1}, $\beta = 1 \times 10^{-11}$ m^{-1} s^{-1} and $f = 8 \times 10^{-4}$ s^{-1}, $\beta = 0.8 \times 10^{-11}$ m^{-1} s^{-1}. (c, d) Time and zonal mean cross-sections for the same two simulations. Colours show potential temperature, grey lines show the zonal wind (CI: 5 and 2 m s^{-1} for $f = 1 \times 10^{-4}$ s^{-1}, $\beta = 1 \times 10^{-11}$ m^{-1} s^{-1} and $f = 8 \times 10^{-4}$ s^{-1}, $\beta = 0.8 \times 10^{-11}$ m^{-1} s^{-1}, respectively) and thin black lines show EKE (CI: 30 and 10 m^2 s^{-2}, respectively). The thick white lines denote the characteristic isentropic slope expected if $\xi = 1$. The bottom figures (c, d) are reproduced from Jansen and Ferrari (2013a).

Table 1. Criticality parameters for all simulations performed.

	$f_0 = 1 \times 10^{-4}$	$f_0 = 2 \times 10^{-4}$	$f_0 = 4 \times 10^{-4}$	$f_0 = 8 \times 10^{-4}$
$\beta = 3.2 \times 10^{-11}$	/	1.2	2.0	4.0
$\beta = 1.6 \times 10^{-11}$	0.9	1.5	2.5	5.5
$\beta = 0.8 \times 10^{-11}$	1.2	2.0	3.8	8.8

interactions. We further find an increasing barotropization, with 97% of the eddy kinetic energy residing in the barotropic mode in the most supercritical simulation.

4.3. The criticality parameter and the vertical structure of the eddy diffusivity

We now analyze the structure of the eddy diffusivity in the model simulations, with the goal of testing the relation between the criticality parameter and the vertical structure of the eddy diffusivity discussed in section 3. We start by focussing on the same two illustrative cases: the marginally critical Earth-like simulation, using $f_0 = 1 \times 10^{-4}$ s^{-1}, $\beta = 1.6 \times 10^{-11}$ m^{-1} s^{-1}, and the strongly supercritical simulation, using $f_0 = 8 \times 10^{-4}$ s^{-1}, $\beta = 0.8 \times 10^{-11}$ m^{-1} s^{-1}.

Figure 6 shows the isentropic eddy PV fluxes and PV gradients as a function of latitude and θ for the two model simulations. In the upper troposphere, the PV fluxes are mostly negative while the PV gradients are mostly positive. Below, the PV fluxes are generally weaker and mostly positive while the PV gradients are mostly negative. Overall, the PV fluxes tend to be down the mean gradient, though the spatial structure of the fluxes and gradients, particularly for the more Earth-like, marginally critical simulation with $f_0 = 1 \times 10^{-4}$ s^{-1} and $\beta = 1.6 \times 10^{-11}$ m^{-1} s^{-1}, shows some exceptions. Most markedly, this simulation reveals a locally very strong PV gradient near the maximum of the zonal jet, which is not reflected by a similar peak in the PV fluxes. This implies a very weak eddy diffusivity near the jet centre, in agreement with the notion that zonal jets can act as diffusivity barriers (Ferrari

and Nikurashin, 2010, and references therein). The suppression of the eddy diffusivity in the upper tropospheric jet has also been discussed by Greenslade and Haynes (2008).

The generally weak PV gradients in the lower troposphere make it difficult to define a local diffusivity from a PV flux/gradient relationship. Nevertheless, we can define bulk diffusivities for the lower and upper troposphere, which are calculated from the vertically integrated eddy PV fluxes and gradients in each layer, as discussed in Appendix A. In agreement with the theoretical arguments above, the layer interface was chosen as the first level above the surface layer (which at each latitude is defined here to include all isentropes up to the 95% quantile of surface potential temperature) where the PV gradient changes sign. Notice that the bulk diffusivity for the lower troposphere includes a contribution associated with the eddy flux and gradient of surface potential temperature, analogous to the PV sheet contribution in continuous QG.

Figure 7 shows the bulk eddy diffusivities in the upper and lower troposphere for the Earth-like simulation with $f_0 = 1 \times 10^{-4}$ and $\beta = 1.6 \times 10^{-11}$, as well as for the most supercritical simulation with $f_0 = 8 \times 10^{-4}$, $\beta = 0.8 \times 10^{-11}$. In agreement with the prediction of Eq. (12), we see that in the Earth-like case, where $\xi \sim 1$, the eddy diffusivity decreases strongly between the lower and upper troposphere. For the simulation with $f_0 = 8 \times 10^{-4}$ and $\beta = 0.8 \times 10^{-11}$, on the other hand, the eddy diffusivity in the lower and upper troposphere is quite similar, in agreement with the criticality parameter being much larger than one.
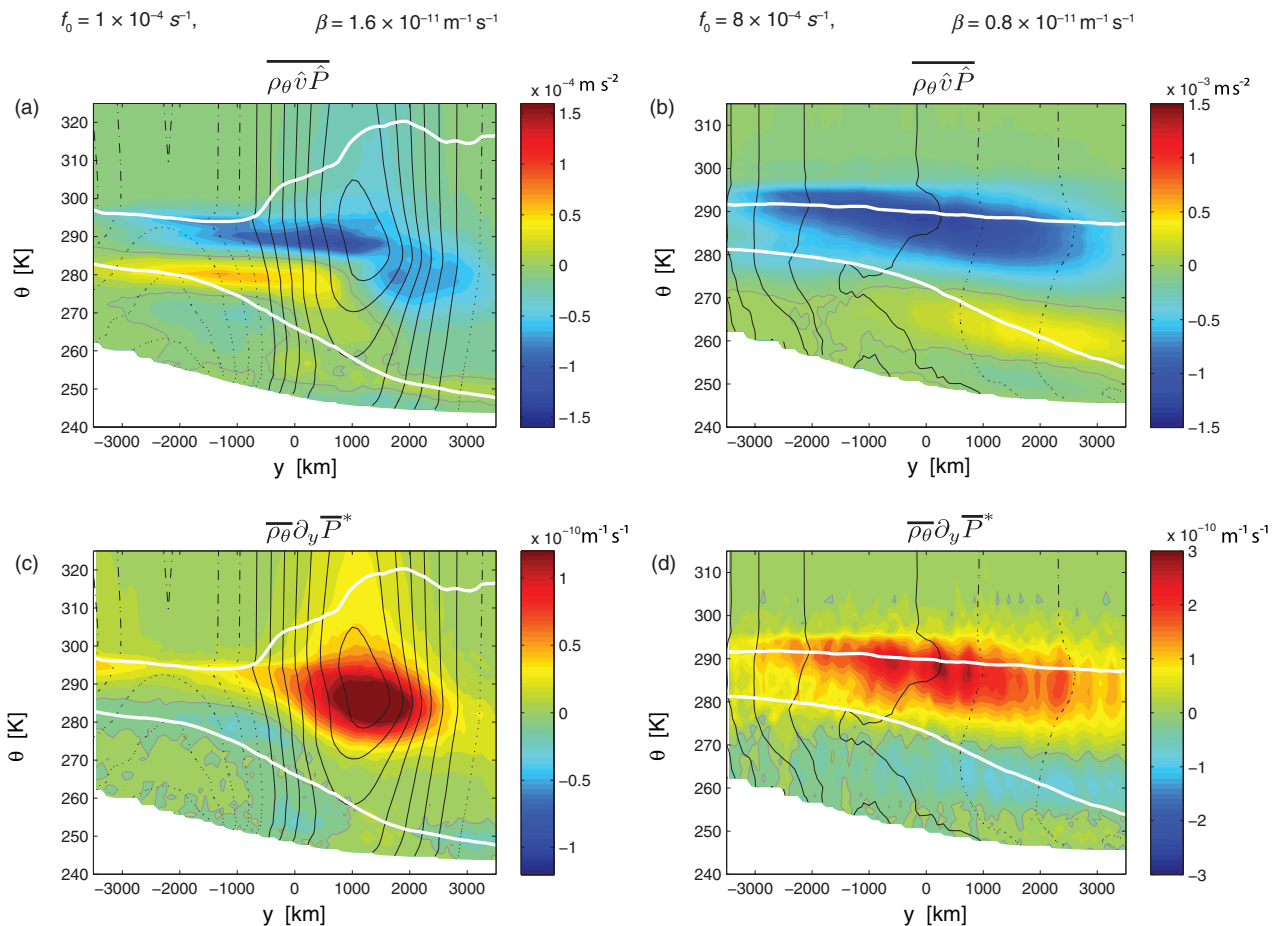
Figure 6. (a, b) Thickness-weighted eddy PV flux for the simulations with $f = 1 \times 10^{-4}\, s^{-1}$, $\beta = 1 \times 10^{-11}\, m^{-1}\, s^{-1}$ and $f = 8 \times 10^{-4}\, s^{-1}$, $\beta = 0.8 \times 10^{-11}\, m^{-1}\, s^{-1}$. (c, d) Corresponding PV gradient for the same two simulations. Grey lines mark the zero contours of the PV fluxes and gradients. The black lines show the thickness-weighted zonal-mean wind $\overline{u}^*$ (CI: 5 and 2 m s^{-1} for $f = 1 \times 10^{-4}\, s^{-1}$, $\beta = 1 \times 10^{-11}\, m^{-1}\, s^{-1}$ and $f = 8 \times 10^{-4}\, s^{-1}$, $\beta = 0.8 \times 10^{-11}\, m^{-1}\, s^{-1}$, respectively). The white lines indicate the top of the surface layer (defined by the 95% quantile of surface potential temperature) and the 'tropopause', used as the top of the upper layer. The 'tropopause' is defined here such that it includes 85% of the northward return flow at any given latitude. Notice that, for the simulation with $f = 1 \times 10^{-4}\, s^{-1}$, $\beta = 1 \times 10^{-11}\, m^{-1}\, s^{-1}$, this 'tropopause' is not very well defined in the northern part of the domain, since the total mass transport is very low. The bulk diffusivities shown in Figures 7 and 8, however, are not very sensitive to the exact choice for the top of the upper layer.

We can test the prediction of the scaling law in Eq. (12) more quantitatively. Figure 8 shows the ratio $[D]/\Delta D$, calculated from horizontal averages of the bulk diffusivities in each layer, against the criticality parameter ξ for all simulations. Following the argument of Nakamura (2008), averaged eddy diffusivities are computed using a harmonic mean, taken over the baroclinically forced region in range $-3500\, km < y < 3500\, km$.** The results are in good agreement with the proposed scaling relation.

5. Conclusions

We used atmospheric reanalysis data to show that eddy PV diffusivity in the Earth's extratropics decreases substantially over the depth of the troposphere. This decrease is in qualitative agreement with the scaling argument in Eq. (12), which suggests that mean states with $\mathcal{O}(1)$ criticality parameters imply that the eddy diffusivity should decay to almost zero at the top of the troposphere, i.e. $\Delta D \sim [D]$.

This relation, which connects the criticality parameter to the vertical structure of the eddy diffusivity, is further supported by a series of numerical simulations using an idealized primitive equation model. Simulations with varying Coriolis parameter f and planetary vorticity gradient β equilibrate into states with a wide range of criticality parameters, spanning about an order of magnitude. The vertical structure of the eddy diffusivity adjusts as predicted: marginally critical mean states are associated with

an eddy diffusivity that decays strongly in the vertical over the depth of the troposphere, while strongly supercritical mean states can have an eddy diffusivity that stays almost constant over the full depth of the troposphere.

The results presented here suggest that any attempt to predict changes in the criticality parameter requires an understanding of what sets the eddy diffusivity and its vertical structure. Unfortunately, no theory exists to predict the vertical structure of the eddy diffusivity without prior knowledge of the criticality of the equilibrated state. In Jansen and Ferrari (2013a), we argue that scaling laws can instead be derived for the magnitude of the eddy diffusivity in the lower troposphere. Together with an additional constraint from the thermodynamic budget, these can be used to predict the criticality from external parameters.

In agreement with two-layer quasi-geostrophic turbulence theory (Held and Larichev, 1996), the changes in the criticality parameter are associated not only with a change in the vertical structure of the eddy diffusivity but also with strong overall changes in the nonlinear flow characteristics. States with criticality parameters close to one are associated with weakly nonlinear flows, where the dominant eddy scale is close to the scale of the most linearly unstable mode. Strongly supercritical states are instead associated with highly nonlinear flows, which exhibit eddies much larger than the scale of the instability, maintained by an inverse energy cascade. This confirms the results of Jansen and Ferrari (2012), where we first showed evidence for this relationship between the criticality parameter and the energy cascade range in multilevel primitive equation models, albeit over a considerably smaller range of criticalities.

**Using arithmetic averages yields somewhat more noisy results, but does not affect the overall picture.
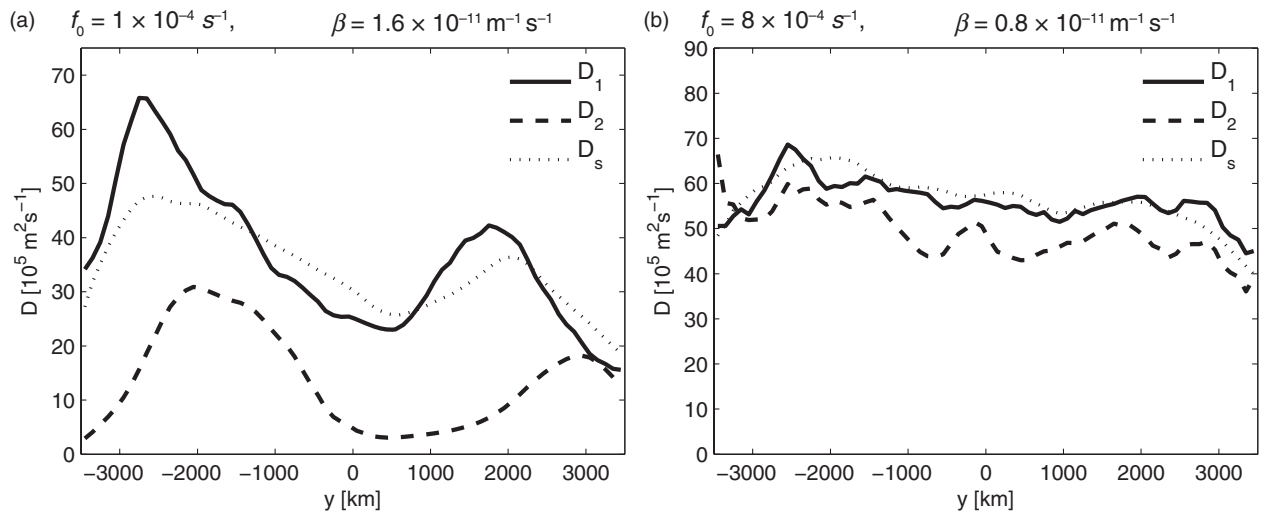
Figure 7. Eddy diffusivities for the simulations with (a) $f = 1 \times 10^{-4}\,\text{s}^{-1}$, $\beta = 1 \times 10^{-11}\,\text{m}^{-1}\,\text{s}^{-1}$ and (b) $f = 8 \times 10^{-4}\,\text{s}^{-1}$, $\beta = 0.8 \times 10^{-11}\,\text{m}^{-1}\,\text{s}^{-1}$. The solid lines show the bulk eddy diffusivity in the lower troposphere and the dashed lines show the bulk eddy diffusivity in the upper troposphere. For comparison, the dotted line shows the eddy diffusivity of surface potential temperature. As found in Jansen and Ferrari (2013b), the latter is overall similar to the bulk diffusivity in the lower layer. All diffusivities have been smoothed by a 500 km running mean.
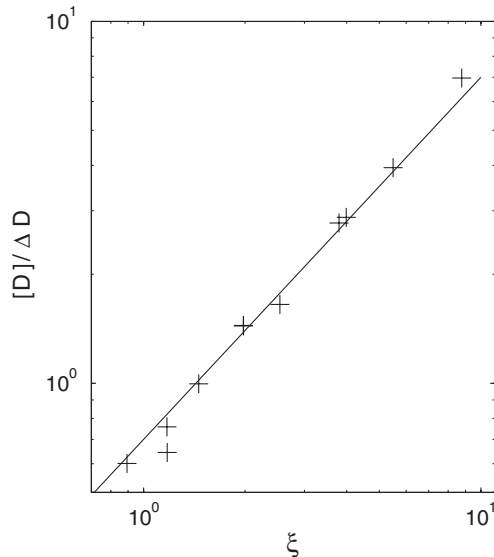

Figure 8. The ratio of the vertical mean of eddy diffusivity to its vertical decrease, $[D]/\Delta D$, against the criticality parameter, ξ. Each marker represents one simulation. The black line denotes $[D]/\Delta D = 0.7\xi$.

Some uncertainty remains as to how relevant these results are to the Earth's atmosphere, because many processes have been neglected. Most notable amongst these are boundary-layer effects and the impact of water-vapour phase changes, which can render dry isentropic PV a poorly conserved quantity unsuitable for a diffusive closure. However, the evidence from atmospheric reanalysis showing that the eddy diffusivity decreases with height suggests that the theoretical arguments hold at least qualitatively.

Acknowledgements

Appendix A: The vertical structure of the eddy diffusivity in primitive equations

Jansen and Ferrari (2013b) show that the primitive-equation, isentropic zonal momentum budget can be used to derive a scaling relation between the vertical structure of the eddy diffusivity and the criticality parameter similar to the relation in Eq. (12). The results will be summarized in the following. The Rossby number is assumed to be small, consistent with QG theory, and appropriate for large-scale atmospheric flows, but no assumption is made for small isentropic slopes.

As in the QG argument presented in the main article, the troposphere is divided into two layers, separated by a potential temperature level $\theta = \theta_1$, which may be a function of latitude. For simplicity, the level separating these two layers is assumed to be above the surface layer (SL), which, at any given latitude, is defined to include all isentropes that intersect with the surface at some time or longitude. We thus have that $\overline{\mathcal{H}(\theta_1 - \theta_s)} = 1$, where θ_s is the surface potential temperature and $\mathcal{H}$ the Heaviside function.

Bulk diffusivities D_1 and D_2 for each layer can formally be defined as the ratio between a weighted integral of the eddy flux of PV and the weighted integral of the PV gradient. For the upper layer, D_2 is defined as

$$D_2 = -\frac{\int_{\theta_1}^{\theta_t} \frac{\overline{\rho_\theta \hat{v} \hat{P}}^*}{\overline{P}^*}\,\mathrm{d}\theta}{\int_{\theta_1}^{\theta_t} \frac{\bar{\rho}_\theta \partial_y \overline{P}^*}{\overline{P}^*}\,\mathrm{d}\theta}, \tag{A1}$$

where θ_t denotes the potential temperature at the tropopause.

The lower layer diffusivity, D_2, includes an additional contribution from the eddy flux and gradient of surface potential temperature and can be written as

$$D_1 = -\frac{\int_{\theta_{\min}}^{\theta_1} \frac{\overline{\rho_\theta \hat{v} \hat{P}}^* + \delta(\theta - \overline{\theta_s}) f \overline{v'\theta'}^s}{\overline{P}^*}\,\mathrm{d}\theta}{\int_{\theta_{\min}}^{\theta_1} \frac{\overline{\rho_\theta \partial_y \overline{P}^* + \delta(\theta - \overline{\theta}^s) f \partial_y \overline{\theta}^s}}{\overline{P}^*}\,\mathrm{d}\theta}, \tag{A2}$$

where $\theta_{\min}$ denotes the minimum potential temperature in the domain, $(\;)^s$ denotes the zonal average along the surface and $(\;)'$ indicates deviations thereof. The surface contribution in the lower layer is analogous to the 'surface PV sheet', which can be used to

treat inhomogeneous boundary conditions in the continuously stratified QG model (Bretherton, 1966). Notice, however, that in isentropic coordinates this surface contribution affects the momentum budget on all isentropes within the SL. It can be reformulated in terms of a surface potential temperature flux only after integrating over the entire SL (Koh and Plumb, 2004; Schneider, 2005).

As in the QG case, one can then derive a scaling relation for the criticality parameter:

$$\xi \sim \frac{fs}{\beta H} \sim \frac{[D]}{\Delta D}, \tag{A3}$$

where, as before, $[D] \equiv \left([\bar{p}^s - \bar{p}(\theta_1)]D_1 + [\bar{p}(\theta_1) - \bar{p}(\bar{\theta}_t)]D_2 \right) / [\bar{p}^s - \bar{p}(\bar{\theta}_t)]$ denotes the vertical mean of the eddy diffusivity, $\Delta D \equiv D_1 - D_2$ the vertical decay, $s \equiv \partial_y|_\theta \bar{z}(\theta_1)$ the isentropic slope and $H \equiv -\overline{\partial_p z}(\theta_1) \left(\bar{p}^s - \bar{p}(\bar{\theta}_t) \right)$ a measure of the tropopause height. The scaling relation in Eq. (A3) is analogous to the QG result in Eq. (12).

As for the QG case, there is some freedom in how to choose the layer interface θ_1. The bulk diffusivities shown in this article are calculated choosing θ_1 as the first isentropic level above the surface layer (for practical purposes, defined as the layer where $\overline{\mathcal{H}(\theta - \theta_s)} < 0.95$) where the PV gradient becomes positive. This level typically separates layers of equatorward mass transport from layers of poleward mass transport. The top of the upper layer, θ_t, is here defined such that it includes 85% of the northward return flow at any given latitude. This threshold was chosen to give rough agreement with the average height of the tropopause as found from a stratification condition. The general results presented in this article, however, do not depend on the exact choice of this threshold.

Finally, it should be noted that, consistent with the derivation in Jansen and Ferrari (2013b), the PV in the numerical simulations is approximated by the planetary PV, $P = f/(g^{-1}\partial_\theta p)$. One exemption to this is the inclusion of the curvature of the barotropic mean flow in the calculation of the PV gradient (i.e. we use an effective planetary vorticity gradient $\beta^* = \beta + \partial_{yy}\bar{u}_t$). While the latter has little influence on the domain-wide averages, it can have a significant effect locally in simulations that develop a strong jet. All additional neglected contributions to the full PV flux and gradient are generally smaller.

Appendix B: Turbulent flow characteristics and the criticality parameter

The criticality parameter is related to characteristics of the turbulent flow itself. Held and Larichev (1996) argue that the flow field in marginally critical mean states is expected to be dominated by weakly nonlinear eddies with a scale close to that of the fastest growing linearly unstable mode (which in turn is of the same order as the Rossby radius of deformation). Large criticality parameters, on the other hand, are expected to be associated with strongly turbulent flows. The dominant eddy scale in the turbulent flow regime scales with the Rhines scale L_R, which in turn becomes much larger than the scale of the most unstable mode by a factor of the same order as the criticality parameter. While eddy kinetic energy (EKE) is still produced near the Rossby radius of deformation, nonlinear eddy–eddy interactions produce an upscale energy transfer to the Rhines scale.

The relation between the criticality parameter and the characteristics of the turbulent flow can be tested by analysis of the spectral EKE budget. We again want to focus on the simulation with Earth-like parameters ($f_0 = 1 \times 10^{-4}\,\text{s}^{-1}$, $\beta = 1.6 \times 10^{-11}\,\text{m}^{-1}\,\text{s}^{-1}$), as well as the most supercritical simulation ($f_0 = 8 \times 10^{-4}\,\text{s}^{-1}$, $\beta = 0.8 \times 10^{-11}\,\text{m}^{-1}\,\text{s}^{-1}$). Figure B1 shows the spectral conversion of eddy available potential energy to eddy kinetic energy (EKE), as well as the spectral dissipation of EKE, for both cases. The eddy energy conversion rate is calculated from the cospectrum between the eddy vertical velocity and potential temperature, as

$$T_{PK} = -\alpha \, \Re \left(\hat{w}'^* \hat{\theta}' \right), \tag{B1}$$

where α is the thermal expansion coefficient, $\hat{()}$ denotes the horizontal Fourier transform of the respective variable and $()^*$ denotes the complex conjugate. Due to the use of a constant linear drag, the eddy kinetic energy dissipation is simply proportional to the eddy kinetic energy itself and can be calculated as

$$D = -\frac{r}{2} \left(|\hat{u}'|^2 + |\hat{v}'|^2 \right), \tag{B2}$$

where $|\,|$ denotes the absolute value. In both cases, spectral energy transfer rates are calculated in two-dimensional spectral space at each vertical level and are afterwards integrated in the vertical and along circles of constant total horizontal wave number.
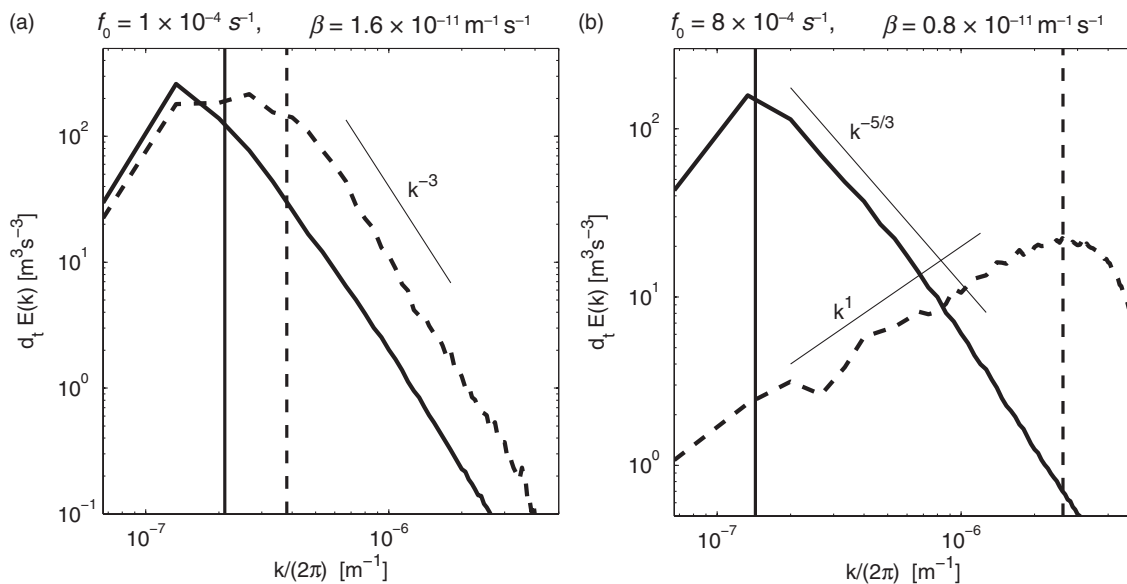

Figure B1. Spectral EKE production and dissipation for the simulations with (a) $f = 1 \times 10^{-4}\,\text{s}^{-1}$, $\beta = 1 \times 10^{-11}\,\text{m}^{-1}\,\text{s}^{-1}$ and (b) $f = 8 \times 10^{-4}\,\text{s}^{-1}$, $\beta = 0.8 \times 10^{-11}\,\text{m}^{-1}\,\text{s}^{-1}$. The figure shows the eddy APE to EKE transfer (dashed) and the EKE dissipation (solid), which is here directly proportional to the EKE itself (due to the use of a linear drag). The vertical dashed and solid lines denote estimates of the wavelength of the most unstable mode and the Rhines scale, respectively (see text).

We also computed the scale of the fastest growing baroclinically unstable mode and the Rhines scale. The wavelength of the most unstable mode is calculated by solving the QG linear stability analysis, as in Smith (2007), based on the meridional planetary QGPV gradient, averaged over the baroclinically forced region in range $-3500\,\mathrm{km} < y < 3500\,\mathrm{km}$. The Rhines wavelength is calculated as

$$L_R \equiv 2\pi\, EKE_t^{1/4}\beta^{-1/2}\,, \qquad (B3)$$

where EKE_t denotes the barotropic EKE.

The spectral EKE budgets, together with the scales of the most unstable mode and the Rhines scales, for the two simulations are shown in Figure B1. In both simulations, the transfer from availalable potential energy to EKE peaks near the wavelength of the most unstable mode as calculated from the QG instability analysis. For the simulation with Earth-like parameters, this instability scale is of the same order as the Rhines scale and the dominant barotropic eddy scale. Only a small upscale energy transfer is observed. This is in agreement with the expected characteristics for a flow near marginal criticality. For the strongly supercritical simulation with $f_0 = 8 \times 10^{-4}\,\mathrm{s}^{-1}$ and $\beta = 0.8 \times 10^{-11}\,\mathrm{m}^{-1}\,\mathrm{s}^{-1}$, the transfer from available potential energy to EKE again peaks near the wavelength of the most unstable mode. The latter, however, is now more than an order of magnitude smaller than the Rhines scale, which in turn again coincides with the dominant barotropic eddy scale. The EKE (and associated dissipation) at this much larger scale must be maintained by a strong upscale energy flux due to eddy–eddy interactions.

The different characteristics of the turbulent flow are also evident in the different slopes of the EKE spectra in Figure B1. The EKE spectrum in the Earth-like simulation falls off as $\sim k^{-3}$ at scales smaller than the dominant eddy scale, as observed in the atmosphere (e.g. Boer and Shepherd, 1983). The EKE in the strongly supercritical simulations, instead, falls off less steeply, with a slope close to $k^{-5/3}$, which is the slope predicted by QG turbulence theory for the inverse energy cascade range (e.g. Rhines, 1979).

References

Birner T, Thompson DWJ, Shepherd TG. 2013. Up-gradient eddy fluxes of potential vorticity near the subtropical jet. *Geophys. Res. Lett.* **40**: 5988–5993, doi: 10.1002/2013GL057728.

Boer GJ, Shepherd TG. 1983. Large-scale two-dimensional turbulence in the atmosphere. *J. Atmos. Sci.* **40**: 164–184.

Bretherton FP. 1966. Critical layer instability in baroclinic flows. *Q. J. R. Meteorol. Soc.* **92**: 325–334.

Ferrari R, Nikurashin M. 2010. Suppression of eddy mixing across jets in the southern ocean. *J. Phys. Oceanogr.* **40**: 1501–1519.

Green JSA. 1970. Transfer properties of the large-scale eddies and the general circulation of the atmosphere. *Q. J. R. Meteorol. Soc.* **96**: 157–185.

Greenslade MD, Haynes PH. 2008. Vertical transition in transport and mixing in baroclinic flows. *J. Atmos. Sci.* **65**: 1137–1157.

Haynes P, Shuckburgh E. 2000. Effective diffusivity as a diagnostic of atmospheric transport 2. Troposphere and lower stratosphere. *J. Geophys. Res.* **105**: 22 795–22 810, doi: 10.1029/2000JD900092.

Held IM. 1978. The vertical scale of an unstable baroclinic wave and its importance for eddy heat flux parameterizations. *J. Atmos. Sci.* **35**: 572–576.

Held IM. 1982. On the height of the tropopause and the static stability of the troposphere. *J. Atmos. Sci.* **39**: 412–417.

Held IM, Larichev VD. 1996. A scaling theory for horizontally homogeneous baroclinically unstable flow on a beta plane. *J. Atmos. Sci.* **53**: 946–952.

Jansen M, Ferrari R. 2012. Macroturbulent equilibration in a thermally forced primitive equation system. *J. Atmos. Sci.* **69**: 695–713.

Jansen M, Ferrari R. 2013a. Equilibration of an atmosphere by adiabatic eddy fluxes. *J. Atmos. Sci.* **70**: 2948–2962.

Jansen M, Ferrari R. 2013b. The vertical structure of the eddy diffusivity and the equilibration of the extratropical atmosphere. *J. Atmos. Sci.* **70**: 1456–1469.

Kållberg P, Simmons A, Uppala S, Fuentes M. 2004. 'The ERA-40 archive', ECMWF ERA-40 Project Report Series, No. 17. European Centre for Medium Range Weather Forecasts: Reading, UK.

Koh TY, Plumb RA. 2004. Isentropic zonal average formalism and the near-surface circulation. *Q. J. R. Meteorol. Soc.* **130**: 1631–1653.

Marshall J, Hill C, Perelman L, Adcroft A. 1997. Hydrostatic, quasi-hydrostatic, and nonhydrostatic ocean modeling. *J. Geophys. Res.* **102**: 5733–5752, doi: 10.1029/96JC02776.

Nakamura N. 1996. Two-dimensional mixing, edge formation, and permeability diagnosed in area coordinates. *J. Atmos. Sci.* **53**: 1524–1537.

Nakamura N. 2008. Sensitivity of global mixing and fluxes to isolated transport barriers. *J. Atmos. Sci.* **65**: 3800–3818.

Oort AH, Peixóto JP. 1983. Global angular momentum and energy balance requirements from observations. In *Theory of Climate*, Saltzman B. (ed.) Advances in Geophysics **25**: 355–490. Elsevier.

Rhines PB. 1977. The dynamics of unsteady currents. In *The Sea*, Goldberg E, McCane I, Brien JJO, Steele JH. (eds.) **6**: 189–318. John Wiley and Sons: New York, NY.

Rhines PB. 1979. Geostrophic turbulence. *Ann. Rev. Fluid Mech.* **11**: 401–441.

Salmon R. 1978. Two-layer quasi-geostrophic turbulence in a simple special case. *Geophys. Astrophys. Fluid Dyn.* **10**: 25–52.

Salmon R. 1980. Baroclinic instability and geostrophic turbulence. *Geophys. Astrophys. Fluid Dyn.* **15**: 167–211.

Schneider T. 2004. The tropopause and the thermal stratification in the extratropics of a dry atmosphere. *J. Atmos. Sci.* **61**: 1317–1340.

Schneider T. 2005. Zonal momentum balance potential vorticity dynamics, and mass fluxes on near-surface isentropes. *J. Atmos. Sci.* **62**: 1884–1900.

Schneider T, Walker CC. 2006. Self-organization of atmospheric macroturbulence into critical states of weak nonlinear eddy–eddy interactions. *J. Atmos. Sci.* **63**: 1569–1586.

Smith KS. 2007. The geography of linear baroclinic instability in Earth's oceans. *J. Mar. Res.* **65**: 655–683.

Stone PH. 1978. Baroclinic adjustment. *J. Atmos. Sci.* **35**: 561–571.

Zurita-Gotor P. 2008. The sensitivity of the isentropic slope in a primitive equation dry model. *J. Atmos. Sci.* **65**: 43–65.

Zurita-Gotor P, Vallis GK. 2010. Circulation sensitivity to heating in a simple model of baroclinic turbulence. *J. Atmos. Sci.* **67**: 1543–1558.

Zurita-Gotor P, Vallis GK. 2011. Dynamics of midlatitude tropopause height in an idealized model. *J. Atmos. Sci.* **68**: 823–838.